3684 *Chem. Mater.* **2009,** *21,* 3684–3692
DOI:10.1021/cm901243a

CHEMISTRY OF MATERIALS
Article

Mössbauer Spectroscopy and Magnetic Measurements As Complementary Techniques for the Phase Analysis of FeP Electrodes Cycling in Li-Ion Batteries

S. Boyanov,[†] M. Womes,[†] L. Monconduit,*[,†] and D. Zitoun*[,†,‡]

[†]*Institut Charles Gerhardt, AIME, Université Montpellier II, Place E. Bataillon, 34095 Montpellier, France, and* [‡]*Department of Chemistry and Center for Nanomaterials of the Institute for Nanotechnology, Bar Ilan University, Ramat Gan, Israel*

Received May 5, 2009. Revised Manuscript Received June 8, 2009

Iron phosphide (FeP) anodes react with lithium through a conversion reaction $FeP + 3Li = Li_3P + Fe°$, leading to nanosized Fe° particles embedded in a Li_3P matrix. Electrochemical tests coupled to ^{57}Fe Mössbauer spectroscopy and magnetic measurements confirm the previously proposed reaction mechanism and complete the investigation of the electrodes by gaining information on the Fe nanoparticles size and surface state from magnetic measurements. More importantly, combining Mössbauer spectroscopy and magnetic measurements appears to be a powerful tool to characterize electrode materials and to give better insights into the complex lithiation−delithiation processes.

Introduction

Recent efforts for the design of new negative electrode materials for Li-ion batteries have led to the screening of binary compounds MP_x exhibiting high gravimetric and volumetric capacities.[1−3] Among them, FeP has been recently investigated both experimentally and by first-principles calculations.[4] According to this study, the electrochemical mechanism for FeP during the first discharge is characterized by the conversion to a composite electrode consisting of metallic nanosized particles embedded in a Li_3P matrix. The reaction can be described as $FeP + 3Li \rightarrow Li_3P + Fe$. Furthermore, it was deduced that this conversion reaction of the first discharge is followed in further cycles by two successive reversible processes labeled A (A′) and B (B′) in the charge (discharge) run. However, although the B process is highly reversible, the A process at lower potential presents a rapid decrease in the reversibility upon cycling. Upon limiting the voltage to the range 2.2−0.2 V, i.e., to the B (B′) process, the electrode displays an interesting longevity, leading to a capacity retention of 300 mA h g^{-1} and 1900 mA h cm^{-3} after 100 cycles, and corresponds to the formation of an intermediate LiFeP phase.[4]

From first-principles phase diagram calculations at $T = 0$ K, it was proposed to associate the A and B′ processes to the formation of an intermediate tetragonal LiFeP phase. Although the previous study, by combining in situ X-ray diffraction, high-resolution transmission electron microscopy (HRTEM), selected area electron diffraction (SAED), and theoretical data, clearly revealed the presence of the conversion products Li_3P and Fe nanoparticles, it failed in (i) providing quantitative experimental data on the amount of Fe formed, (ii) characterizing the LiFeP-intermediate phase and (iii) identifying the phases present in the charged electrode. The open questions about FeP are thus related to the nature of the electrode from the middle to the end of the charge process and to the relative amounts of the various phases formed during a cycle.

From a general point of view, the reaction of a starting material with lithium is often accompanied by an amorphization. The final reaction product, and also intermediate phases formed during the lithiation/delithiation process, are obtained either as well-crystallized particles, but with extremely low particle diameters of a few nanometers,[5] or as poorly organized matter.[6] In both cases, no diffraction pattern allowing a phase analysis will be obtained.

Among alternative techniques not requiring any long-range order, X-ray absorption spectroscopy gains increasing importance.[7] The technique has, however, some serious restraints. Usually, it requires the use of synchrotron radiation, available only at a few large scale research

*Corresponding author. E-mail: laure.monconduit@univ-montp2.fr (L. M.); zitoun@univ-montp2.fr (D.Z.).

(1) Bichat, M. P.; Politova, T.; Pascal, J. L.; Favier, F.; Monconduit, L. *J. Electrochem. Soc.* **2004**, *151*(12), A2074–A2081.
(2) Souza, D. C. S.; Pralong, V.; Jacobson, A. J.; Nazar, L. F. *Science* **2002**, *296*, 2012.
(3) Gillot, F.; Bichat, M.-P.; Favier, F.; Morcrette, M.; Doublet, M.-L.; Monconduit, L. *Electrochim. Acta* **2004**, *49*(14), 2325.
(4) Boyanov, S.; Bernardi, J.; Gillot, F.; Dupont, L.; Womes, M.; Tarascon, J. M.; Monconduit, L.; Doublet, M. L. *Chem. Mater.* **2006**, *18*, 3531.
(5) Larcher, D.; Prakash, A. S.; Laffont, L.; Womes, M.; Jumas, J. C.; Olivier-Fourcade, J.; Hedge, M. S.; Tarascon, J. M. *J. Electrochem. Soc.* **2006**, *153*, A1778.
(6) Dedryvère, R.; Denis, S.; Lippens, P. E.; Olivier-Fourcade, J.; Jumas, J. C. *J. Power Sources* **2001**, *204*, 97–98.
(7) Chadwick, A. V.; Savin, S. L. P.; Fiddy, S.; Alcantara, R.; Lisbona, D. F.; Lavela, P.; Ortiz, G. F.; Tirado, J. L. *J. Phys. Chem. C* **2007**, *111*, 4636–4642.

 Published on Web 07/17/2009

facilities. The study of electrode materials prepared in the home laboratory bears the risk of sample alteration by relaxation phenomena during the transport to the synchrotron. On-site in situ measurements are difficult, especially at low cycling rates, because of limitations in beam time and because of the complexity of the sample holder needed to avoid air contact.

We therefore chose two experimental techniques readily accessible in our laboratory, ^{57}Fe Mössbauer spectroscopy and measurements of magnetic susceptibilities. Mössbauer spectroscopy provides information on the local environment of the probing nucleus, independently of the presence of long-range order. Magnetic measurements give insight in the magnetic behavior of all the phases (mainly ferromagnetic and antiferromagnetic), with information on the nature, morphology, and surface state of the nanoparticles.

The combined use of these two techniques for the analysis of electrode materials is still rather unusual. In the literature, one article reports on the use of magnetic measurements to follow an electrochemical degradation of a Sn/Co anode.[8] In this study, the amorphous starting materials were converted to cobalt nanoparticles in the blocked (ferromagnetic) and the superparamagnetic states with a mean diameter of 3.6 nm. The total fraction of ferromagnetic Co increases up to 49% at the 10th cycle. In the case of metal phosphides, a single study reports on the formation of superparamagnetic nanoparticles upon cycling from FeP_2.[9] The data collected did not allow the authors concluding about the nature of the magnetic phase: Fe or Fe_xP ($x = 1$, 2 or 3).[10]

The purpose of the present article is thus 2-fold: (i) It is intended to show what information the combined use of magnetic measurements and Mössbauer spectrocopy can furnish on sample morphology and composition. (ii) The methodology is applied to the study of the electrochemical mechanism in FeP, which will reveal the redox mechanism occurring in the cycling of the FeP/Li cell and confirm the formation of a ternary LiFeP-like phase during cycling.

Experimental Section

Sample Preparation. The orthorhombic FeP ($Pna2_1$) and ternary phase LiFeP ($P4/nmm$) were synthesized from stoichiometric mixtures of powders of the elements (Fe, Alfa Aesar, 350 mesh, 99.9%; P, Alfa Aesar, 100 mesh, 99%; Li, 99.9%, Goodfellow) in evacuated silica or stainless steel ampules at high temperature according to previously reported procedures.[4,11,12] The ternary phase was carefully washed with deionized water to remove any Li_3P impurity.

Electrochemical Tests. Electrochemical discharge and charge runs were carried out in Swagelok test cells connected to a VMP or a MacPile automatic cycling and data recording system (Biologic Co., Claix, France). The cells were assembled in a glovebox under argon and comprised a lithium metal disk as the negative electrode, a Whatman GF/D borosilicate glass fiber sheet saturated with a solution of 1 M $LiPF_6$ in ethylene carbonate/dimethyl carbonate (1:1 by weight) as the electrolyte, and a mixture of the iron phosphide with 15 weight percent carbon black (SP) as the positive electrode. Usually, 10−12 mg of mixed iron phosphide and carbon black were used in the tests which were carried out at $C/5$ or $C/10$ scan rates (1 Li per formula unit in 5 or 10 h) in a potential window between 2.5 and 0.0 V versus Li^+/Li^0.

Sample Characterization. X-ray diffraction (XRD) on the starting material FeP and on LiFeP was performed on a Philips X'Pert diffractometer using Cu Kα radiation.

Magnetic properties were measured on a Superconducting Quantum Interference Design (SQUID) magnetometer MPMS XL7 between 2 and 300 K in magnetic fields between 0 and 5 T. The temperature dependent susceptibility was measured using a DC procedure. The sample was first cooled to 2.0 K under zero magnetic field, then data were recorded in a low magnetic field of 5 mT between 2 and 300 K (zero-field-cooled, ZFC). Field-cooled (FC) measurements were performed from 2 to 300 K after cooling the sample in an applied field. Measurements on electrode materials were carried out ex situ, after extraction of the electrode material from the Swagelok cell. The results are given with respect to the effective mass of iron contained in the sample, after correction for added carbon black and inserted lithium.

Mössbauer spectra were recorded in the constant acceleration mode and in transmission geometry on a standard Mössbauer spectrometer composed of components from Ortec and Wissel. A ^{57}Co(Rh) source with a nominal activity of 370 MBq was used. Low temperature spectra were recorded by cooling the sample in a flow cryostat from L'Air Liquide, using liquid nitrogen or liquid helium as cooling agent. The source was always kept at room temperature. The hyperfine parameters isomer shift (δ), quadrupole splitting (ΔE_q), quadrupolar perturbation (ε') and hyperfine magnetic field (H) of the various species were determined by fitting Lorentzian lines to the experimental data, using the ISOfit program.[13] Distributions of magnetic hyperfine fields were calculated with a program created by LeCaër and Dubois.[14] Field distributions were simulated by a total of 70 subspectra covering field strengths from 6 to 35 T with field-independent isomer shift δ and quadrupolar perturbation ε'. The intensities p of these magnetic subspectra are given in the form of a distribution function $p(H)$. Isomer shifts are given with respect to the center of the six-line spectrum of an α-Fe foil recorded at room temperature. Mössbauer spectra of electrode materials were recorded ex situ after transferring the material under argon atmosphere from the Swagelok cell to a specific airtight sample holder equipped with windows transparent for γ radiation. Each spectrum along the discharge/recharge cycle was recorded on a separate, individual sample.

Results

In Figure 1, we present the voltage−composition profile of the FeP/Li cell, the first derivative, and the associated in situ X-ray diffraction data recorded on first

(8) Tamura, N.; Kato, Y.; Mikami, A.; Kamino, M.; Matsuta, S.; Fujitani, S. *J. Electrochem. Soc.* **2006**, *153*(8), A1626.
(9) Silva, D. C. C.; Crosnier, O.; Ouvrard, G.; Greedan, J.; Safa-Sefat, A.; Nazar, L. F. *Electrochem. Solid-State Lett.* **2003**, *6*(8), A162.
(10) Silva, D. C. C. Ph.D. Thesis, University of Waterloo, Waterloo, ON, **2006**
(11) Franke, W.; Meisel, K.; Juza, R. *Z. Anorg. Allg. Chem.* **1934**, *218*, 346–59.
(12) Juza, R.; Langer, R. *Z. Anorg. Allg. Chem.* **1968**, *361*, 58.
(13) Kündig, W. *Nucl. Instr. Methods Phys. Res.* **1969**, *75*, 336.
(14) LeCaër, G.; Dubois, J. M. *J. Phys. E* **1979**, *12*, 1083.

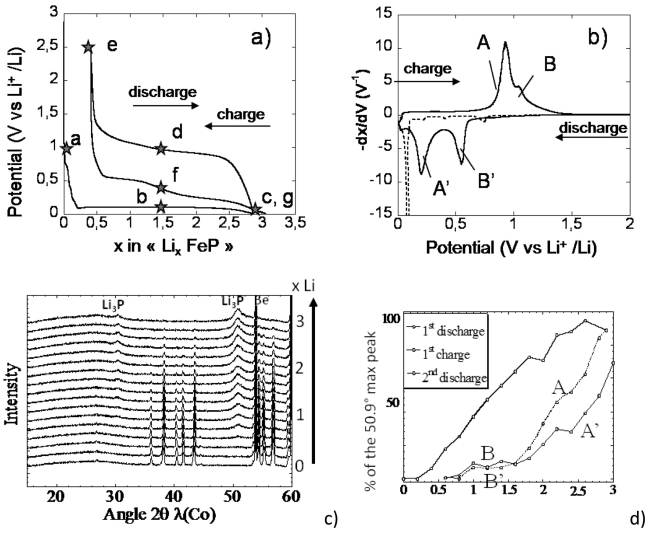

Figure 1. (a) Potential−composition profile of a FeP electrode versus lithium, plotted as the electrochemical potential vs the number x of lithium atoms inserted; (b) derivative $-dx/dV$ vs potential; dashed line, first discharge; solid line, first charge and second discharge; (c) in situ XRD collected for the FeP/Li cell for the first discharge;[4] Bragg reflections are indicated for Li_3P; (d) Li_3P surface peak integration of the Li_3P (110)/(103) characteristic peaks for the first and second discharge and the first charge, plotted as a function of x.

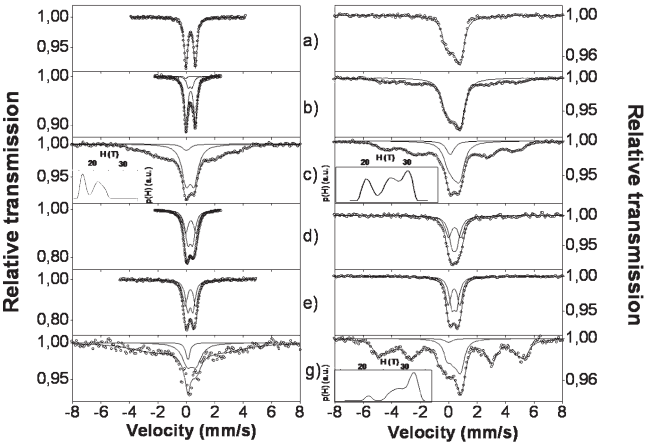

Figure 2. Mössbauer spectra recorded on FeP electrodes at various depths of lithiation: (a) starting material, (b) 1.5 Li (half discharge), (c) 2.8 Li (complete discharge), (d) 1.3 Li (half recharge), (e) 0.8 Li (complete recharge), (g) 2.8 Li (second complete discharge). Left column, spectra recorded at room temperature; right column, spectra recorded at 77 K. Inserts show distributions of magnetic fields p(H) (see text for details).

discharge. As mentioned in the introduction of this paper, the two electrochemical processes proposed for the second and following cycles are

$$\mathrm{B(B')} : \mathrm{FeP} + \mathrm{Li} \leftrightarrow \mathrm{LiFeP}$$

$$\mathrm{A(A')} : \mathrm{LiFeP} + 2\mathrm{Li} \leftrightarrow \mathrm{Li_3P} + \mathrm{Fe}$$

To identify and quantify (i) the amount of Fe formed during the biphasic conversion process on first discharge and (ii) to quantitatively follow the oxidation reaction of Fe upon charge, a series of samples was collected at different depths of discharge/charge of the FeP/Li half cell, labeled a−g in Figure 1a. All samples were characterized by Mössbauer spectroscopy and SQUID measurements.

^{57}Fe Mössbauer Spectroscopy. Figure 2 shows on the left-hand side a series of ^{57}Fe Mössbauer spectra recorded at room temperature at different stages of discharge and charge runs, while the right-hand side shows for each sample the corresponding spectrum obtained at liquid nitrogen temperature. The spectra are labeled in accordance with Figure 1a. The hyperfine parameters of all samples are given in Table 1. The systematic increase of all isomer shifts by about 0.1 mm/s when going from 295 to 77 K is due to the relativistic second-order Doppler effect.[15] Spectrum a corresponds to the starting material FeP. Isomer shift δ and quadrupole splitting ΔE_q of the doublet obtained at room temperature agree well with data from the literature.[16] The low-temperature spectrum can be fitted by a single sextet with a weak hyperfine field of 3.4 T and a quadrupolar perturbation ε' of −0.08 mm/s, supposing identical magnetic field strengths for all iron atoms in the lattice. This refinement does not exactly reflect the effective magnetic structure of FeP which is more complicated,[17] and characterized by a larger number of iron sites with different local magnetic field strengths (see ref 18 for the magnetic structure and ref 15 for high-resolution Mössbauer spectra and a discussion on their correct refinement). However, our refinement reproduces well the spectral shape on this large velocity scale (which has been chosen such that the magnetic splitting of metallic iron of 10.9 mm/s between the outermost lines at 77 K can be observed) and will thus be appropriate and sufficient for our purpose, which is to determine the spectral weight of magnetically ordered FeP.

The spectra of Figure 2b were recorded after the insertion of 1.5 Li during the first discharge. The room temperature spectrum consists mainly of the doublet of FeP. In addition, a weak doublet with isomer shift δ = 0.27 mm/s and quadrupole splitting ΔE_q = 0.27 mm/s is seen. Such a signal was already observed in ref 4 and was attributed to a ternary, LiFeP-like phase, after theoretical considerations had shown that such a phase could be easily formed by electrochemical insertion of Li into FeP.[4] We synthesized LiFeP with the aim of obtaining its hyperfine parameters, not previously reported in the literature, and obtained it with minor impurities of Fe_2P and Li_3P revealed by XRD. Figures 3a and 3b show the Mössbauer spectra recorded at 295 and 77 K, respectively. In the refinement of the room temperature spectrum, the hyperfine parameters δ and ΔE_q as well as the intensity ratio between the two doublets of Fe_2P were fixed to the values reported in the literature.[19] At both

(15) Pound, R. V.; Rebka, G. A., Jr. *Phys. Rev. Lett.* **1960**, *4*, 274. Josephson, B. D. *Phys. Rev. Lett.* **1960**, *4*, 341.
(16) Häggström, L.; Narayanasamy, A. *J. Magn. Magn. Mater.* **1982**, *30*, 249.
(17) Felcher, G. P.; Smith, F. A.; Bellavance, D.; Wold, A. *Phys. Rev. B* **1971**, *3*, 3046.
(18) Felcher, G. P.; Smith, F. A.; Bellavance, D.; Wold, A. *Phys. Rev. B* **1971**, *3*, 3046.
(19) Wäppling, R.; Häggström, L.; Rundqvist, S.; Karlsson, E. *J. Solid State Chem.* **1971**, *3*, 276.

Table 1. Hyperfine Parameters of the Phases Observed during Discharge and Charge of FeP[a]

		295 K					77 K					
sample on Figures 1/2	Li atoms	δ (mm/s)	ΔE_q or ε' (mm/s)	2Γ (mm/s)	H (T)	spectral weight (%)	δ (mm/s)	ΔE_q or ε' (mm/s)	2Γ (mm/s)	H (T)	spectral weight (%)	identification
a	0.0	0.31(1)	0.66(1)	0.29(1)	0	100	0.41(1)	−0.08(1)	0.61(2)	3.4	100	FeP
b	1.5	0.31(1)	0.66(1)	0.29(1)[b]	0	80	0.39(1)	−0.07(1)	0.70(1)	3.6	69	FeP
		0.27(2)	0.27(1)	0.29(2)[b]	0	18						Li_xFeP
		− 0.04(9)	0.00	0.22[c]	0	2						Fe (sp)
							0.23(5)	− 0.01(2)	1.53(9)	28	31	Fe (m)
c	2.8	0.27[c]	0.67[c]	0.65[c]	0	10	0.42[c]	0.59[c]	0.65[c]	0	9	FeP (p/sp)
							0.42	−0.08[c]	0.65[c]	3.6	14	FeP (m)
		0.25[c]	0.29[c]	0.65[c]	0	22	0.39[c]	0.29[c]	0.65[c]	0	15	Li_xFeP
		0.00[c]	0.00[c]	0.65[c]	0	5	0.15[c]	0.00[c]	0.73	0	2	Fe (sp)
		0.00	0.00	0.70[c]	[d]	63	0.15[c]	0.00[c]	0.70[c]	[d]	60	Fe (m)
d	1.5	0.30(1)	0.67(1)	0.39(1)[b]	0	58	0.42(2)	0.87(4)	0.56[b]	0	46	FeP (p/sp)
		0.25(1)	0.32(1)	0.39(1)[b]	0	42	0.40(2)	0.32(3)	0.56[b]	0	54	Li_xFeP
e	0.4	0.30(1)	0.66(1)	0.42(1)[b]	0	63	0.38(1)	0.81(1)	0.44(1)[b]	0	50	FeP (p/sp)
		0.27(1)	0.31(1)	0.42(1)[b]	0	37	0.39(1)	0.34(1)	0.44(1)[b]	0	50	Li_xFeP
g	3.0	0.38[c]	0.64[c]	0.87[c]	0	32	0.46[c]	−0.08[c]	0.60[c]	3.1	19	FeP (m)
		0.10[c]	0.00	0.33[c]	0	6	0.10[c]	0.00[c]	0.70[c]	0	4	Fe (sp)
		0.06[c]	0.00[c]	3.4(9)	19	62	0.16[c]	0.00[c]	0.70[c]	[d]	77	Fe (m)

[a] Quadrupole splitting ΔE_q is given for paramagnetic samples ($H = 0$) and the quadrupolar perturbation ε' for magnetically split spectra ($H \neq 0$ or field distribution). The magnetic properties are indicated as static magnetism (m) or paramagnetic/superparamagnetic (p/sp). [b] Parameters constrained to be equal. [c] Parameter kept fixed in the refinement. [d] Field distribution; see inset in Figure 2.

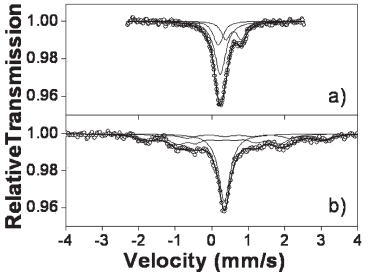

Figure 3. Mössbauer spectra of LiFeP recorded at (a) 295 and (b) 77 K. Fe_2P is present as an impurity. See text for details.

temperatures, the spectrum of the ternary phase could be fitted with a single line, in agreement with the perfect tetrahedral environment of iron in LiFeP,[4,11] with isomer shifts $\delta_{295K} = 0.24(7)$ mm/s and $\delta_{77K} = 0.35(1)$ mm/s and full line widths at half-maximum $2\Gamma_{295K} = 0.38(2)$ mm/s and $2\Gamma_{77K} = 0.39(1)$ mm/s. We thus attribute the aforementioned doublet of electrode b, despite the nonzero quadrupole splitting, to the formation of a ternary, LiFeP-like phase, where a high amount of surface atoms and eventually the strain caused by interactions with surrounding phases like FeP, Li_3P, or metallic iron prevent the atoms from adopting the highly symmetric arrangements of the bulk material, leading to a small quadrupole splitting. Moreover, the lithium content of this ternary phase might deviate from a supposed stoichiometry $Li_{1.0}FeP$. This phase is constituted of small particles not observable by XRD and will be considered in the following as Li_xFeP. One would expect to find a distribution of quadrupole splittings reflecting the different environments around iron atoms in such an inhomogeneous phase rather than a single doublet from a unique crystallographic site. The increased line width observed for some of the samples might reflect a multitude of sites. The room temperature spectrum of sample b (Figure 2) of the middle of the first discharge reveals furthermore the presence of a weak singlet at zero velocity which is attributed to small particles of superparamagnetic iron. The shape of the low-temperature spectrum is again essentially determined by FeP. However, a magnetically ordered phase with a broad distribution of hyperfine magnetic field strengths on the iron sites begins to appear. The field distribution extends up to 28 T, which is somewhat less than the value of bulk α-Fe of 33.9 T at 77 K (see Table 1). We attribute the reduced field strength and the line broadening to the presence of very small particles of metallic iron with a broad distribution in size. The smaller iron particles have a higher fraction of surface atoms with a reduced number of magnetic neighbors, which leads to lower local magnetic field strengths than in bulk α-Fe.[20] The shape of the low-temperature spectrum does not allow concluding on the presence of a small amount of a ternary phase.

The spectra of Figure 2c were recorded on a fully discharged cell (0 V, 2.8 Li). The room-temperature spectrum shows the doublet of FeP, indicating that full discharge to 0 V does not completely consume the starting material. The spectrum reveals the presence of a magnetically ordered phase with a maximum splitting corresponding to a field of 25 T, which is less than the room-temperature value of bulk α-Fe of 33.0 T. However, the spectrum of this magnetic phase does not show the characteristic six-line structure, but is strongly deformed by dynamic effects, i.e., by the rapid fluctuation of the magnetization vector as it occurs in small, single-domain particles. A six-line spectrum is observed only when the fluctuation rate is low, i.e., when the magnetization vector conserves its orientation for a time that is long as compared to the characteristic measuring time of Mössbauer spectroscopy τ_M. In the present case τ_M is given by the period of the Larmor precession of the nuclear magnetic

(20) Hendriksen, P. V.; Linderoth, S.; Lindgard, P. A. *Phys. Rev. B* **1993**, *48*, 7259. Bodker, F.; Morup, S.; Linderoth, S. *J. Magn. Magn. Mater*. **1995**, *373*, 140–144.

moment of the ^{57}Fe nucleus in the field of 33 T of α-Fe, thus $\tau_M \cong 5 \times 10^{-9}$ s. When on the other hand the fluctuation is fast as compared to τ_M, the six-line splitting then collapses and a single absorption line is obtained. The shape of spectrum 2c effectively suggests the presence of a singlet at $\delta = 0$ mm/s of the smallest iron particles showing such superparamagnetic behavior at room temperature. At 77 K, the fluctuation of the magnetization in the iron particles is strongly slowed down and the six-line structure of the spectrum becomes visible. The lines are strongly broadened, reflecting the wide distribution of local magnetic fields on the iron sites. The distribution has its maximum at 28 T and extends up to 33 T, which is very close to the value of 33.9 T of bulk α-Fe at 77 K. Comparison of spectra b and c shows that the spectral weight of metallic iron at 77 K is higher for sample c than for b, in agreement with a continuous transformation of FeP to Li_3P and Fe^0 during the first discharge. Furthermore, the magnetic field distribution of c extends to higher values than for b. The magnetic ordering becomes visible already at room temperature for c in contrast to b, indicating that not only more iron is formed at the end of the discharge, but also that the particle size has increased. The shape of the low-temperature spectrum in Figure 2c suggests further that at this stage the residual FeP leads not only to the magnetically split spectrum observed for the starting material but also to a doublet with $\delta =$ 0.42 mm/s and $\Delta E_q = 0.59$ mm/s. Apparently, the transformation of FeP to metallic iron and Li_3P has reduced the size of the remaining FeP particles in such a way that an important fraction of FeP shows now superparamagnetic behavior. The spectral shapes of sample c at both temperatures suggest also that the initially formed small amount of Li_xFeP persists until the end of the discharge.

The spectra of Figure 2d were recorded after recharge to 1 V of a fully discharged cell. The room temperature spectrum can be fitted with two doublets associated with FeP and the ternary Li_xFeP phase. The low-temperature spectrum of sample d reveals no magnetically ordered metallic iron. Moreover, the shape of the spectrum suggests that the residual FeP is now entirely present as superparamagnetic small particles.

The spectra of Figure 2e were recorded on a fully recharged cell. The same two phases FeP and Li_xFeP are observed as for d, but the amount of the ternary phase is reduced as compared to sample d, whereas that of FeP has increased. No metallic iron is observed at 77 K. FeP is present only as superparamagnetic small particles.

Sample f at the middle of the second discharge (spectra not shown in Figure 2) contains FeP and the ternary phase together with a few percent of metallic iron. The spectra labeled g in Figure 2 were recorded at the end of the second discharge. The room temperature spectrum shows again the singlet of superparamagnetic small iron particles together with the strongly broadened sextet of larger particles. At low temperature, a strongly broadened, magnetically split sextet is observed. The distribution of local magnetic fields extends up to 34 T (i.e., the value of bulk α-Fe) and has a maximum at 32 T. The spectral shape suggests the presence of a small amount of superparamagnetic iron even at 77 K. Residual FeP is clearly distinguished at both temperatures, in paramagnetic form at room temperature and magnetically ordered at 77 K. The complexity of the spectra does not allow concluding unambiguously on the presence of a ternary phase at this stage.

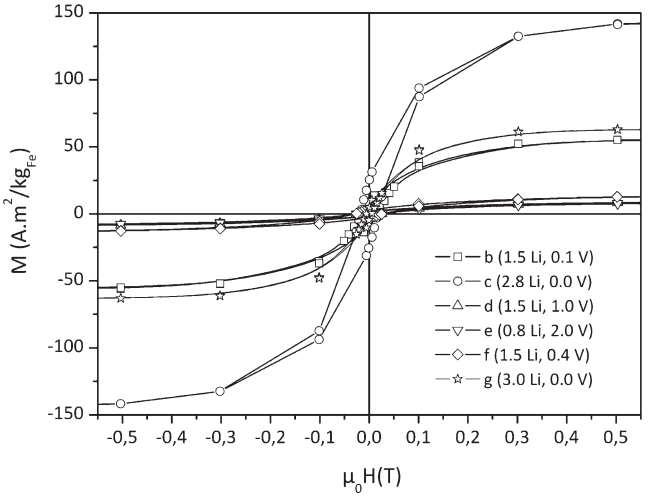

Figure 4. Field dependence at 2 K of the magnetization of a FeP electrode at various depths of lithiation during (b, c) first discharge, (d, e) first recharge, and (f, g) second discharge.

Magnetic Measurements. Measurements of the saturation magnetization at 2 K were carried out for the quantitative detection of metallic iron. The size of the iron particles was deduced from the blocking temperature of the magnetization determined by comparison of the zero-field-cooled and field-cooled (ZFC/FC) magnetic susceptibilities, according to the procedure described by Respaud et al.[21] The field dependence of the magnetization at different depths of lithiation of the FeP electrode material measured at 2 K is shown in Figure 4. Hysteresis loops are observed for all samples (see insert in Figure 5). The nonzero coercive field and remanent magnetization indicate a ferromagnetic behavior.

The saturation magnetization M_s of the starting material FeP at 2 K is 6.2 A m^2/kg$_{Fe}$ (not shown in Figure 4). FeP has been determined by neutron diffraction to be a paramagnetic compound with an helical antiferromagnetism below 125 K.[16] Our material displays a magnetic moment slightly higher than expected because of traces of Fe_2P as secondary phase, which is ferromagnetic below 215 K.[22] The reaction of FeP with lithium during the first discharge leads to a progressive increase of the saturation magnetization (Figure 4), reaching 57.5 A m^2/kg$_{Fe}$ at half discharge (sample b in Figure 4, 1.5 Li inserted at 0.1 V vs Li^+/Li) and 150 A m^2/kg$_{Fe}$ at full discharge (c, 2.8 Li, 0 V). The high magnetization value at 2.8 Li can be compared

(21) Respaud, M.; Broto, J. M.; Rakoto, H.; Fert, A. R.; Thomas, L.; Barbara, B.; Verelst, M.; Snoeck, E.; Lecante, P.; Mosset, A.; Osuna, J.; Ely, T. O.; Amiens, C.; Chaudret, B. *Phys. Rev. B* **1998**, *57*, 2925.
(22) Wäppling, R.; Häggström, L.; Ericsson, T.; Devanarayanan, S.; Karlsson, E.; Carlsson, B.; Rundqvist, S. *J. Solid State Chem.* **1975**, *13*, 258.

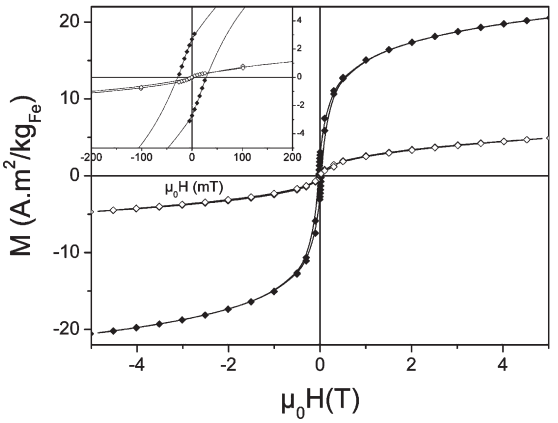

Figure 5. Field dependence of the magnetization of a FeP electrode after half of the second discharge (sample f) recorded at 2 K (filled squares) and 300 K (open squares); inset shows details of the coercive field.

to the known values for bulk α-Fe (219 A m^2/kg), Fe_3O_4 (92 A m^2/kg_{Fe}), and γ-Fe_2O_3 (76 A m^2/kg_{Fe}). The experimental value allows us to conclude on the effective formation of iron particles and to exclude an accidental oxidation of the sample during analysis. Obviously, the amount of metallic iron in the electrode grows progressively during the first electrochemical process, at the end of which at least 75% of the pristine material is transformed to metallic iron, assuming that the electrochemically formed iron carries a magnetic moment close to the bulk value.

Recharging the battery from 0 to 1 V, which corresponds to process A, leads to a strong decrease of the saturation magnetization (c and d). The iron content falls down to 7%. This magnetization is very weak compared to that of sample b and confirms the occurrence of an electrochemical process correlated with the formation of LiFeP from Li_3P+Fe. The amount of LiFeP cannot be determined by magnetic measurements since the paramagnetic signal from LiFeP is shadowed by the ferromagnetic contribution of the remaining iron. No further decrease of the magnetization is observed during process B between 1 and 2 V (e).

The second discharge is first characterized by a quite unchanged magnetization during the B′ process up to 1.5 Li from 12.6 A m^2/kg_{Fe} in sample e to 20.5 Am^2/kg_{Fe} in the sample f. Moreover this latter value is very low compared to that of sample b of the first discharge at the same lithium content. It is fully consistent with the main formation of LiFeP from the charged electrode (B′ process) during the second discharge. The second part of the second discharge is characterized by a new drastic increase of the magnetization correlated to the Fe formation (sample g). According to the magnetic measurements, the electrochemical process displays a large discrepancy between the first and the second discharge. Nevertheless, metallic iron is formed in both first and second discharge.

The magnetization curves at room temperature and at 2 K obtained at the middle of the second discharge are plotted in Figure 5. At room temperature, the sample exhibits superparamagnetic behavior, as deduced from the zero coercive field and the zero remanent magnetization (see insert in Figure 5). The appearance of superparamagnetism is the result of the small particle size (less than the critical size for single domain particles) and the high degree of dispersion of iron in the Li_3P matrix, leading to magnetically isolated Fe nanoparticles. At 2 K, the magnetization vectors are blocked and a ferromagnetic behavior is observed, characterized by a coercive field of 28 mT and a remanent magnetization M_r = 2.7 A m^2/kg_{Fe} (M_r/M_s = 0.11)

ZFC/FC measurements of the magnetic susceptibilities were carried out with the aim to gain more information about the radii of the superparamagnetic iron particles and about the transition from ferromagnetic to superparamagnetic behavior of the system during the electrochemical process. The ZFC curves show a maximum susceptibility value at the blocking temperature (T_B). Figure 6 clearly shows the dependence of T_B upon cycling and thus the size evolution of Fe particles through the electrochemical cycle. At the end of the first discharge (Figure 6a), the ZFC-FC curve shows a ferromagnetic behavior with a blocking temperature above 300 K, indicating properties close to bulk α-Fe and particle radii exceeding 7.1 nm. For all other analyzed points of the electrochemical cycle, the ZFC curves evidence a blocking temperature between 10 and 20 K corresponding to particle sizes around 3 nm. Figure 6b shows as an example the curves obtained for sample f at the middle of the second discharge. The maximum of the particle size distribution determined from fits of the ZFC-FC curves is listed in Table 2. A volume distribution (log-normal, $f(v)$) was determined from fits of the magnetic ZFC/FC curves and allowed the determination of a magnetic size (see Table 2). Using these size values, we can well-reproduce the experimental curves, and especially the distribution of blocking temperatures, without introducing a distribution of anisotropy constants (fixed at the bulk value) or of spontaneous magnetizations (obtained from high field measurements). The distribution of blocking temperatures ($f(T_B)$) can be thus only ascribed to the volume distribution ($f(v)$).[21] For instance, Figure 6b shows a fit of the ZFC/FC curve for sample f at the middle of the second discharge (E = 0.4 V). At low temperature, the experimental FC deviates from the model due to some magnetic dipolar interactions not described by the calculation. We deduced the size of the Fe nanoparticles as $r = 3.1 \pm 0.4$ nm. The size of the Fe particles is almost constant for samples d, e, f.

Discussion

The magnetic measurements confirm the previous theoretical and experimental data with the formation of iron nanoparticles during the conversion process on first discharge. The small particles radii obtained from fitting the ZFC/FC explain why XRD does not show the formation of α-Fe. The most interesting feature lies in the very low variation of Fe particles size ($r = 3 \pm 0.5$ nm) during the first part of the discharge. Once the conversion voltage

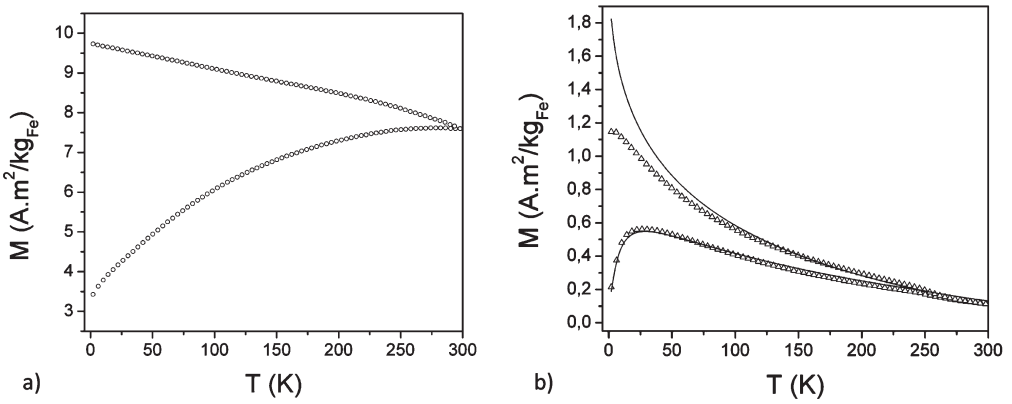

Figure 6. Magnetic susceptibilities of FeP electrodes at different depths of lithiation under a magnetic field of $\mu_0 H = 5.0$ mT: (a) sample c, end of first discharge; (b) sample f, half of second discharge; recorded under both ZFC and FC conditions.

Table 2. Magnetic Moment at Saturation (M_{sat}) and Remanant (M_r) and Coercive Fields (H_C) Deduced from the High Field Measurements[a]

composition; voltage	H_c (2 K) (mT)	M_r (2 K) (A m^2/kg$_{Fe}$)	M_{sat} (2 K) (A m^2/kg$_{Fe}$)	%Fe	T_B (K)	r_{mean} (nm)	σ (nm)	K_v (J/m^3)
a FeP	0	0	6.2	0				
b 1.5 Li; 0.1 V	16	9.2	57.5	30.5	94	4.8		7×10^4
c 2.8 Li; 0 V	17	24	150	75.2	> 300	> 7.1		7×10^4
d 1.5 Li; 1 V	25	1.6	12.6	7.4	12	2.9	0.5	7×10^4
e 0.4 Li; 2 V	26	1.7	12.6	7.2	12	3.1	0.5	7×10^4
f 1.5 Li; 0.4 V	28	2.7	20.5	11.8	14	3.1	0.4	7×10^4
g 3.0 Li; 0 V	17	10.1	65	32.6	> 300	> 7.1		7×10^4

[a] Metallic iron percentage deduced from the magnetization assuming a "dead magnetic layer" (see discussion for details). Fe nanoparticles size deduced from fitting the ZFC/FC curves.

plateau (at 0.1 V) is over (see Figure 1), the particle size grows to give a blocking temperature above room temperature at 2.8 Li. The size dependence is typical of a two steps behavior: (a) formation of isolated superparamagnetic nanoparticles homogeneous in size and dispersed in a matrix consisting of FeP, LiFeP, and Li_3P; (b) beginning coalescence or agglomeration of iron particles, which leads to a ferromagnetic material at the end of the discharge. As pointed out in the previous X-ray study,[4] the hypothesis of agglomerates is more likely. Therefore, at the end of the discharge, the materials would consist of 3 nm particles in strong magnetic interactions.

As shown below from the literature, for particles in this range of size, all studies but one report on a magnetic moment per atom lower than the bulk, which would be due to a surface passivation. Assuming the bulk crystallographic phase and a spherical shape, a particle with a radius of 2.9 nm contains 5000 atoms, divided in 76% core atoms and 24% surface atoms.

The magnetic studies of Fe nanoparticles attracted a considerable interest in the 1980s and 1990s. The magnetic moment and anisotropy are closely related to the size and dimensionality (shape) of the nanostructures. Theoretically, the magnetic properties will strongly depend on the surface to volume atomic ratio and on the change in crystallographic phase that is induced by the size reduction.[23] This effect has been observed experimentally on clusters prepared by time-of-flight methods with an enhanced magnetic moment below a cluster nuclearity of 600 Fe atoms,[24] and more recently from organometallic precursors.[25] Nevertheless, any ligand adsorption has proven to significantly affect the magnetizm of naked Fe clusters, carbonyl withdraws most of the moment from the outer shell of the clusters.[26]

Besides clusters in the gas phase, iron nanoparticles have been produced by a variety of chemical routes: mechanical milling from bulk materials,[27] decomposition of iron pentacarbonyl,[28] iron amides,[29] and iron carboxylates.[30] Obviously, all these syntheses lead to iron nanoparticles stabilized by a ligand shell. As previously demonstrated, the ligand shell diminishes, in the case of carboxylates, or drastically counterbalances the magnetic moment, in the case of carbonyl, from the surface atoms even without any air exposure. With the notable exception of iron amide precursor, all chemical routes lead to magnetizations much lower than the bulk value $M_S = 223$ emu g^{-1}. The magnetization values range between 80 and 170 emu g^{-1} for a mean particle diameter of 7 nm.

(23) Bobadova-Parvanova, P.; Jackson, K. A.; Srinivas, S.; Horoi, M. *Phys. Rev. B* **2002**, *66*, 195402.
(24) Billas, I. M. L.; Châtelain, A.; de Heer, W. A. *Science* **1994**, *265*, 1662.
(25) Lacroix, L. M.; Lachaize, S.; Falqui, A.; Blon, T.; Carrey, J.; Respaud, M.; Dumestre, F.; Amiens, C.; Margeat, O.; Chaudret, B.; Lecante, P.; Snoeck, E. *J. Appl. Phys.* **2008**, 103.
(26) Pick, S.; Dreysse, H. *Phys. Rev. B* **1999**, *59*, 4195.
(27) Rosensweig, R. E. *AIAA J.* **1966**, *4*, 1751.
(28) (a) Suslick, K. S.; Fang, M.; Hyeon, T. *J. Am. Chem. Soc.* **1996**, *118*, 11960. (b) Park, S.-J.; Kim, S.; Lee, S.; Khim, Z. G.; Char, K.; Hyeon, T. *J. Am. Chem. Soc.* **2000**, *122*, 8581. (c) Nikitenko, S. I.; Koltypin, Y.; Palchik, O.; Felner, I.; Xu, X. N.; Gedanken, A. *Angew. Chem., Int. Ed.* **2001**, *40*, 4447.
(29) Dumestre, F.; Chaudret, B.; Amiens, C.; Renaud, P.; Fejes, P. *Science* **2004**, *303*, 821.
(30) Kim, D.; Park, J.; An, K.; Yang, N. K.; Park, J. G.; Hyeon, T. *J. Am. Chem. Soc.* **2007**, *129*, 5812.

This magnetic dead layer seems very difficult to avoid from a solution phase synthesis method and electrochemical methods would not give better results in that sense. Therefore, we would expect to measure a magnetic moment lower than in bulk iron during the electrochemical lithium insertion. The most realistic hypothesis would be to consider that, under the harsh conditions reactions, the surface atoms behave like a dead magnetic layer. The resulting sum would give a magnetization of 200 A m^2 kg^{-1} for a $R = 7.1$ nm particle diameter. The conversion of FeP to Fe would then reach the value of 75.2%, in perfect and quantitative agreement with the Mössbauer study. In Table 2, the values of Fe content takes into account the non magnetic shell surrounding the particles. One may then notice the discrepancy between the first discharge and the further cycles, in perfect agreement with a two-step mechanism with the formation of LiFeP.

Figure 7 resumes the results found by the various techniques for the first two cycles of FeP. It shows, from top to bottom, the ratio Li_xFeP/FeP derived from the Mössbauer spectra, the amount of Li_3P detected by in situ XRD (from the area of the main Bragg peak of Li_3P, see figure 1d), the relative amounts of metallic iron determined by both magnetic measurements and Mössbauer spectroscopy, the number of lithium atoms per formula unit of FeP contained in the electrode, and the evolution of the cell potential, all drawn versus time. Values from Mössbauer spectroscopy are based on the spectra obtained at 77 K, where the differences between the *f* factors of recoilless resonant gamma absorption of the various phases should be smaller than at room temperaure. The results clearly demonstrate the simultaneous formation of Li_3P and metallic iron during the first discharge, according to the reaction mechanism $FeP + 3\ Li \rightarrow Li_3P + Fe$ proposed in eq . From the amount of lithium effectively inserted into the sample during the first discharge (2.67 Li, if we deduce 0.13 Li consumed in the early stage of the discharge by reaction with carbon at a potential of 0.75 V, see Figure 1a and b) we expect to find 89% Fe and 11% residual FeP. This value agrees reasonably well with the 75 and 62% found by magnetic measurements and Mössbauer spectroscopy, respectively, if we take into account some sources of uncertainty like, for example, consumption of some lithium for the formation of an unavoidable passivating layer, formation of a small amount of a ternary phase Li_xFeP (approximately 20% according to Mössbauer spectroscopy), or the fact that percentages derived from Mössbauer spectra represent only their spectral weight. Determination of effective relative amounts from Mössbauer spectra would require correction for the individual fractions *f* of recoilless resonant gamma absorption of the various phases (note that the factor *f* of Li_xFeP is unknown).

From these combined analyses, we show that charging the cell to a potential of 1 V vs Li^+/Li (process A, Figure 1), which corresponds to the extraction of approximately 1 Li, results in (i) the almost complete disappearance of Li_3P and metallic iron and (ii) the simultaneous formation of Li_xFeP. Apparently the extraction of a part

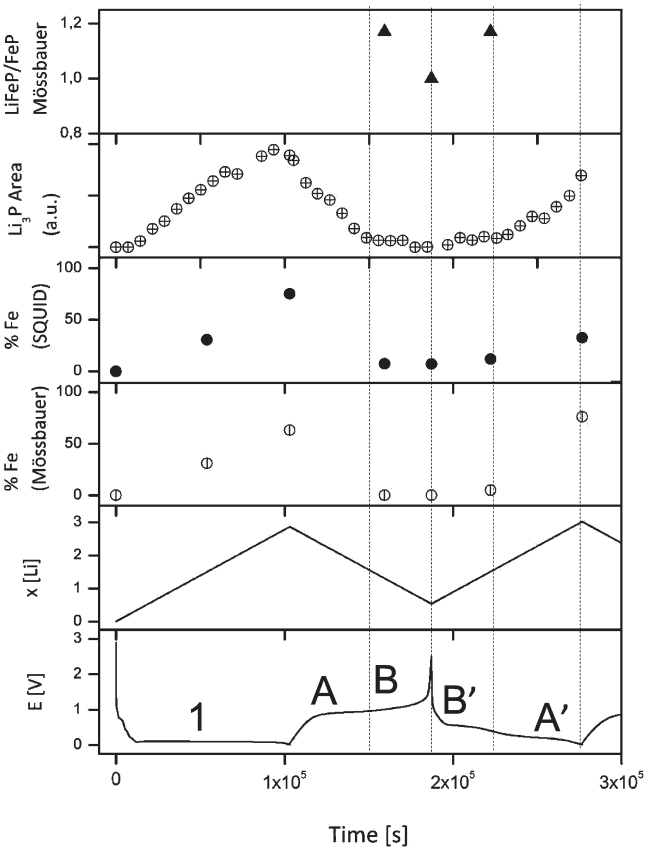

Figure 7. Variation in the Li_xFeP/FeP ratio, the amount of Li_3P, the relative amount of metallic iron determined by both magnetic measurements and Mössbauer spectroscopy, the number of lithium atoms per formula unit FeP, and the evolution of the cell potential of FeP electrodes (from top to bottom), all drawn versus time.

of the lithium atoms from Li_3P destabilizes the remaining matrix in such a way that it favors the reaction with metallic iron to form Li_xFeP according to a net reaction $Fe + Li_3P \rightarrow Li_xFeP$. Further charging up to 2 V (process B) causes the partial disappearance of Li_xFeP and the growth of FeP. As the Mössbauer parameters of this ternary phase and those of FeP remain rather constant over the whole charge/discharge process while only their relative proportions vary, we conclude that process B corresponds to the oxidation of a part of the ternary phase leading back to a FeP lattice with some Li_xFeP remaining. The second discharge to 0.5 V (process B′) leads to the transformation of some FeP to Li_xFeP and is the inverse of process B. Further discharge to 0 V (process A′) again forms Li_3P and metallic iron and is the inverse of process A.

Figure 7 shows clearly that the partial irreversibility of the processes is due to the important stability of the ternary phase Li_xFeP as compared to the end compounds of the cycle, i.e., FeP on the charged side and Li_3P and Fe on the discharged side. This ternary phase is quite easily formed from Li_3P and Fe during the first charge in process A, ending—according to Mössbauer spectroscopy—with a Li_xFeP/FeP spectral ratio of 1.2. However, the further extraction of lithium from Li_xFeP in process B stops already at a Li_xFeP/FeP ratio of approximately 1, which explains partially the capacity loss of the first cycle. Process B′ of the second discharge leads easily back to a

Li_xFeP/FeP ratio of approximately 1.2 like at the beginning of process B, so that a cycle comprising B and B′ alone is highly reversible. The further discharge, transforming Li_xFeP to Li_3P and Fe in process A′, seems to stop before being completed. Unfortunately, the complexity of the Mössbauer spectrum of this point (Figure 2g) allows no reliable determination of the Li_xFeP/FeP ratio. The results from XRD and magnetic measurements in Figure 7 suggest, however, that less Li_3P and metallic iron are formed at the end of the second discharge than at the end of the first. The processes A/A′ are only partially reversible as already demonstrated previously.[4]

The high relative stability of LiFeP was already predicted from thermodynamical considerations.[4] According to this study, the direct formation of a ternary phase already in the first discharge is only hindered by kinetic limitations, i.e., the low diffusion rate of Li^+ ions into the rather large grains of the pristine FeP material. The small amount of Li_xFeP observed by Mössbauer spectroscopy during the first discharge (Figure 2b and 2c) could thus be due to a surface layer formed on the FeP particles. At the end of the first discharge/charge cycle the particle size is found to be reduced from the initial micrometer scale to sizes from several tens to several hundreds of nanometers, which facilitates the complete penetration of the particles by Li^+ ions in the subsequent cycles.

Conclusion

In this article, we have proposed a new method to follow the electrochemical processes. Combining Mössbauer spectroscopy and magnetic measurements is an interesting approach to the analysis of FeP electrode materials because of the different magnetic properties of the involved phases (antiferromagnetic FeP, ferromagnetic iron, paramagnetic Li_xFeP). The two techniques are complementary insofar as measurements of the magnetic susceptibilities allow detecting even small amounts of a ferromagnetic phase like metallic iron, provided all other phases present are dia- or paramagnetic or give only a weak signal from antiferromagnetism. Their detection is possible even in cases where Mössbauer spectroscopy fails to reveal them unambiguously because of overlap with absorption lines of other phases. On the other hand, the presence of a paramagnetic compound like LiFeP—even when X-ray amorphous—is easily demonstrated by Mössbauer spectroscopy.

These methods are very general and could be adapted to the study of numerous systems involving a ferromagnetic transition metal (Fe, Co, or Ni) and a Mössbauer active element (Fe, Ni, Sn, Sb). In the present case, this complementary analysis by Mössbauer spectroscopy and magnetization measurements was a powerfull tool (i) to quantitatively identify 3 nm iron nanoparticles at the end of discharge and (ii) to unambiguously identify the Li_xFeP intermediate phase reversibly formed upon cycling, and the restructured FeP at the end of charge. All these phases are X-ray amorphous. These macroscopic measurements corroborate quantitatively the previously proposed electrochemical mechanism.

To summarize the electrochemical mechanism involved in the FeP/Li half cell, three equations are proposed.

First discharge:

$$FeP + 3Li \rightarrow Li_3P + Fe \quad (60-75\% \text{ complete})$$

First charge/second discharge:

$$Li_3P + Fe \leftrightarrow Li_xFeP \quad (\text{process } A/A' > 90\% \text{ complete})$$

$$Li_xFeP \leftrightarrow FeP + xLi \quad (\text{process } B/B' > 50\% \text{ complete})$$